INT. J. REMOTE SENSING, 1999, VOL. 00, NO. 00, 0000 0000

The Advanced Spaceborne Thermal Emission and Reflection Radiometer (ASTER): data products for the high spatial resolution imager on NASA's EOS-AM1 platform

M. ABRAMS

California Institute of Technology/Jet Propulsion Laboratory 183-501, 4800 Oak Grove Dr., Pasadena, California 91109, USA;
email: mike@lithos.jpl.nasa.gov

(*Received 11 March 1999; in final form 4 July 1999*)

Abstract. The Advanced Spaceborne Thermal Emission and Reflection Radiometer (ASTER) is a high spatial resolution, multispectral imager with along-track stereo capabilities scheduled for launch on the first NASA spacecraft of the Earth Observing System (EOS AM-1) in mid-1999. Data will be obtained in 14 spectral bands covering the visible through the thermal infrared wavelength region. A number of standard data products will be available to requesters through an on-line archival and processing system. Particular, user-specified data acquisitions will be possible through a Data Acquisition Request system.

1. Introduction

Satellite sensors provide the only method to collect global data on a regular basis. NASA's Earth Science Enterprise (ESE) is working with international partners to design, build and launch advanced instruments to observe phenomena related to global change. ESE consists of four parts: (1) a series of satellites called the Earth Observing System (EOS); (2) a series of smaller satellites; (3) a scientific research programme; and (4) an EOS Data and Information System (EOSDIS) that will provide a mechanism for storing and processing the data, and distributing them to the scientific community.

The Advanced Spaceborne Thermal Emission and Reflection Radiometer (ASTER) is a high spatial resolution, multispectral imager with along-track stereo capabilities scheduled for launch on the first NASA spacecraft of the Earth Observing System (EOS AM-1) in mid-1999 (Yamaguchi *et al.* 1998). The ASTER instrument is built by the Japanese Government through MITI (Ministry of International Trade and Industry). The ASTER Science Team consists of Japanese, American and Australian scientists who are responsible for the development of research requirements and algorithms for data reduction and analysis.

Data from ASTER will be used by scientists to study a wide range of problems dealing with the surface of the Earth, including vegetation change due to natural and human causes; monitoring and evaluating natural hazards such as volcanic eruptions; studying short-term climate change and searching for reliable indicators of change, such as retreating or advancing glaciers; monitoring sea ice extent and

International Journal of Remote Sensing
ISSN 0143-1161 print/ISSN 1366-5901 online © 1999 Taylor & Francis Ltd
http://www.tandf.co.uk/JNLS/res.htm
http://www.taylorandfrancis.com/JNLS/res.htm

albedo; observing degradation of coral reefs as indicators of climate change or human effects; improved resource exploration (Abrams and Hook 1995).

To accomplish these tasks, ASTER will provide observations in three spectral regions, as well as stereo observations, using three separate radiometers (table 1). The visible and near-infrared (VNIR) system has three spectral bands covering 0.52–0.86 μm at 15 m resolution; the short wavelength infrared (SWIR) subsystem has six spectral bands covering 1.60–2.45 μm at 30 m resolution; and the thermal infrared (TIR) subsystem has five spectral bands covering 8.125–11.65 μm at 90 m resolution. The VNIR system includes a separate, single spectral band radiometer inclined backward at an angle of 27.6° to provide an along-track stereo capability. The swath width will be 60 km. Cross-track pointing will allow viewing of any spot on Earth a minimum of once every 16 days. A wide dynamic range and selectable multiple gain settings will help ensure useful signal-to-noise for a variety of investigations.

One of ASTER's primary goals is to obtain a cloud-free map of the land surface by the end of the 6-year mission. In addition, specific targets will be observed in response to the science objectives of EOS investigators. The stereo capability will be used to generate high-resolution digital elevation maps. Observations will also include sites involving simultaneous ground measurements; targets of opportunity such as active volcanoes and major weather events; and high resolution observations of clouds.

Table 1. ASTER instrument specifications.

	VNIR	SWIR	TIR
Spatial resolution (m)	15	30	90
Data rate (Mbps)	62	23	4
Cross-track pointing	±24	±8.55	±8.55
Cross-track pointing	±318	±116	±116
Swath width (km)	60	60	60
Quantization (bits)	8	8	12
Stereo	Y	N	N

Wavelength region	Band	Bandwidth (μm)
VNIR	1	0.52 – 0.60
	2	0.63 – 0.69
	3	0.76 – 0.86
SWIR	4	1.60 – 1.70
	5	2.145– 2.185
	6	2.185– 2.225
	7	2.235– 2.285
	8	2.295– 2.365
	9	2.360– 2.430
TIR	10	8.125– 8.475
	11	8.475– 8.825
	12	8.925– 9.275
	13	10.25 –10.95
	14	10.95 –11.65

2. Data architecture

The commitment to make Earth science data easily available to a wide community of users is implemented by EOSDIS. This is a comprehensive data and information system (Price *et al.* 1994) providing a range of services: user support; data archive management and distribution; information management; product generation; spacecraft command and control; and data capture and telemetry.

Data products that are generated routinely for spatially and/or temporally extensive subsets of the data are called standard data products. For ASTER (and all other EOS instruments) the products are provided in hierarchical data format (HDF), and are defined by level:

Level 0: reconstructed, unprocessed instrument data at full resolution.

Level 1A: reconstructed, unprocessed instrument data at full resolution, time-referenced, and annotated with ancillary information, including radiometric and geometric calibration coefficients and georeferencing parameters, computed and appended but not applied to the Level 0 data.

Level 1B: Level 1A data that have been processed to sensor units.

Level 2: derived geophysical variables at the same resolution and location as the Level 1 source data.

Level 3: variables mapped on uniform space–time grid scales, usually with some completeness and consistency.

Level 4: model output or results from analyses of lower level data, e.g. variables derived from multiple measurements.

3. Standard data products

ASTER will provide the user community with Standard Data Products (table 2). Examples are shown using simulated ASTER data over Death Valley, California. The simulated dataset was created using co-registered Airborne Visible and Infrared Imaging Spectrometer aircraft data (Green *et al.* 1988) for the visible through the SWIR region; and Thermal Infrared Multispectral Scanner aircraft data (Palluconi and Meeks 1985) for the TIR. The two datasets were co-registered, resampled to the proper ASTER instrument response functions for each spectral band, and spatially resampled to 15, 30 or 90 m resolution, depending on the wavelength region. The images cover an area of about 15 × 60 km. (These data and images are available on-line from http://asterweb.jpl.nasa.gov). cleared

Table 2. ASTER standard data products.

Level	Product
1A	radiance at sensor
1B	registered radiance at sensor
2	decorrelation stretch
2	brightness temperature
2	surface radiance-VNIR, SWIR
2	surface radiance-TIR
2	surface reflectance-VNIR, SWIR
2	surface kinetic temperature
2	surface emissivity
4	Digital Elevation Model

3.1. *Level 1 products*

The Level 1A data product consists of the image data, the radiometric coefficients, the geometric coefficients, and the auxiliary data (Fujisada 1998). The data are produced from raw Level 0 data. Data are separated by telescope (VNIR, SWIR and TIR), and put into band sequential (BSQ) format. The radiometric coefficients are determined from pre-launch engineering measurements, and post-launch engineering and vicarious calibration determinations. The coefficients can be used to convert digital numbers in the Level 0 data to calibrated radiance at the sensor. In the TIR, on-board blackbody observations are used to calibrate the TIR signals. A wide range of geometric correction parameters are determined and stored as geometric coefficients. These include spacecraft attitude vectors, inter-telescope registration, intra-telescope band-to-band registration, etc. All of these factors are included in the Level 1A product, but they are not applied to the data. The data are reported in units of digital counts or digital numbers (DN), scaled to 8 bits. This form of data may be required by users who do not want their data resampled in any way, and need to analyse ASTER data in as raw a state as possible.

The Level 1B data are generated from the Level 1A data by applying the radiometric coefficients to calibrate the data to radiance-at-the-sensor; and by applying the geometric coefficients to produce the map projection requested by the user. These data are reported in units of radiance ($W\,m^{-2}\,sr^{-1}\,\mu m^{-1}$). The user can also select the resampling method used for both of these transformations. This format is the one most users will probably order who want 'raw' ASTER data, rather than derived higher level data products.

3.2. *Decorrelation stretch*

The decorrelation stretch products are enhanced colour composites of three bands from each of the telescopes (figure 1). The processing algorithm is based on a forward and reverse principal components transformation, whose outputs are the original three bands with increased colour saturation (Soha and Shwartz 1978, Gillespie *et al.* 1986). For the VNIR data (figure 1, left), bands 3, 2 and 1 are displayed in red (R), green (G) and blue (B), respectively; for the SWIR (figure 1, centre), bands 8, 6 and 4 are displayed in RGB; for the TIR (figure 1, right), bands 14, 12 and 10 are displayed in RGB. The images have been spatially resampled to their proper ASTER pixel sizes of 15, 30 or 90 m for the VNIR, SWIR and TIR regions, respectively. Bad Water in Death Valley, the lowest place in the United States, is in the bottom middle of the images. The three composites of ASTER data illustrate the different compositional information available in various wavelength regions. For example, the bright red areas in the VNIR image are vegetation patches at Furnace Creek Ranch and on the Furnace Creek Fan. The turquoise area in the upper left corner of the SWIR image depicts ground covered by limestone fragments. In the TIR image, surfaces with the mineral quartz present are depicted in red.

3.3. *Brightness temperature*

The algorithm that computes brightness temperature uses a pre-computed table of values that represent observed radiance as a function of brightness temperature for a given sensor. The generation and inversion of this table are computationally expensive, but the results are constant for a given wavelength calibration of the sensors, and therefore, presumably, for the life of the mission. The table needs to be generated and inverted only once, prior to launch. Then, to generate the brightness

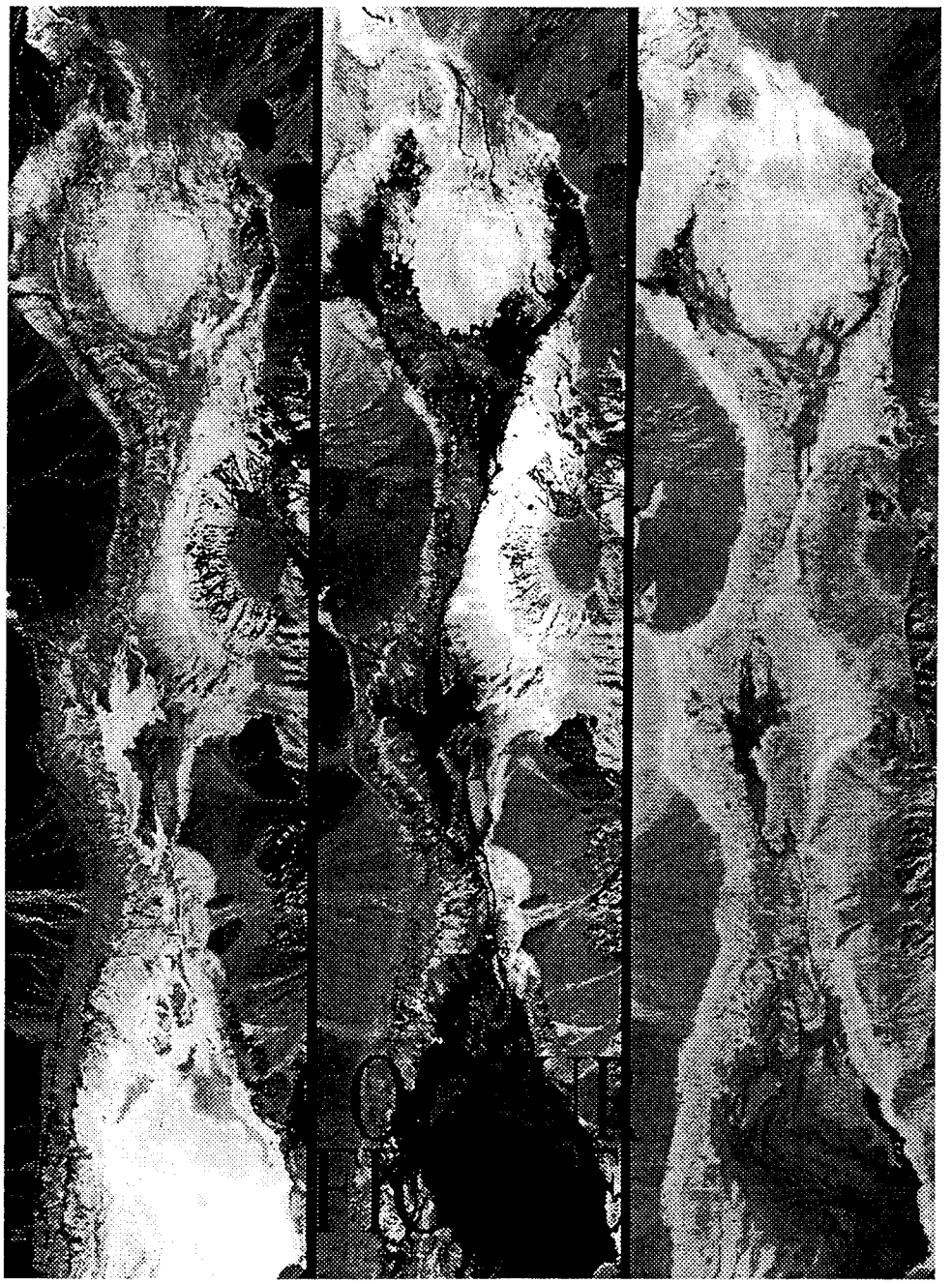

Figure 1. Decorrelation stretch images of simulated ASTER data over Death Valley, California. The left image displays bands 3, 2 and 1 in red, green and blue (RGB), respectively; the spatial resolution is 15 m. The centre image combines bands 8, 6 and 4 in RGB; the spatial resolution is 30 m. The right image combines bands 14, 12 and 10 in RGB; the spatial resolution is 90 m. All three images cover an area of 12 km × 60 km, and were produced from aircraft scanner data.

temperature product for a given scene, one need only use the radiance value of each input pixel as the index to point to the desired brightness temperature in the stored table, and place the table values in the output dataset.

The input dataset for this product is the radiance observed at the sensor, in units of $W m^{-2} sr^{-1} \mu m^{-1}$. The output product is reported in units of degrees centigrade, scaled by a factor of 100. For example, an output value of 2735 implies a brightness temperature of 27.35 degrees. Since the brightness temperature values are stored as 16-bit signed integers, the precision of the brightness temperature values will be 0.01° C. When a brightness temperature product needs to be generated, the task is simply a matter of table lookup.

3.4. *Surface radiance and reflectance-VNIR and SWIR*

The algorithm used to calculate surface radiance (figure 2) and reflectance in the VNIR and SWIR wavelength regions (bands 1–9) relies on deriving a relationship between the surface radiance/reflectance and the top-of-the-atmosphere radiance from information regarding the scattering and absorbing characteristics of the atmosphere. This relationship is used to convert radiances measured by ASTER to surface radiance and reflectance.

The absorbing and scattering characteristics of the atmosphere are planned to be obtained from outside sources. The anticipated sources of this information are results from other AM-1 platform sensors; we also anticipate using global assimilation model results. Difficulties arise when these sources of information are not available. In early versions of the code, climatological data will be used when no atmospheric information are provided. Later versions will offer the user an opportunity to perform an ASTER-only correction.

The atmospheric correction used is based on the calibration and related atmospheric correction work of the Remote Sensing Group of the Optical Sciences Center at the University of Arizona. The calibration work uses the reflectance-based method which has been used since the mid-1980s to radiometrically calibrate Landsat-4 and -5 Thematic Mapper (TM) (Slater *et al.* 1987, and Thome *et al.* 1993). The method relies on ground-based measurements of the surface and atmosphere at a selected site to predict top-of-the-atmosphere (TOA) radiances (Slater *et al.* 1987). Surface measurements are made for a number of pixels by transporting spectroradiometers across a test site and measuring upwelling radiance. This radiance is converted to reflectance by comparing it with measurements from a panel of known reflectance. Solar radiometer data are converted to atmospheric transmittances and used to determine the aerosol properties and columnar absorber amounts over the site (Biggar *et al.* 1990, Thome *et al.* 1992). The results are used as input to a radiative transfer code to predict the TOA radiance. The digital numbers (DNs) reported by the sensor are compared with these predicted radiances to give a radiometric calibration. The radiance product is reported in units of radiance ($W m^{-2} sr^{-1} \mu m^{-1}$); the reflectance product is reported in units of percent reflectance (0–100%).

3.5. *Surface radiance-TIR*

The objectives of the ASTER investigation in the thermal infrared include, among other things, providing estimates of the radiance leaving the land surface (figure 2). The radiance which is measured by the ASTER instrument includes emission, absorption and scattering by the constituents of the Earth's atmosphere. The purpose of the atmospheric correction method is to remove these effects providing estimates of

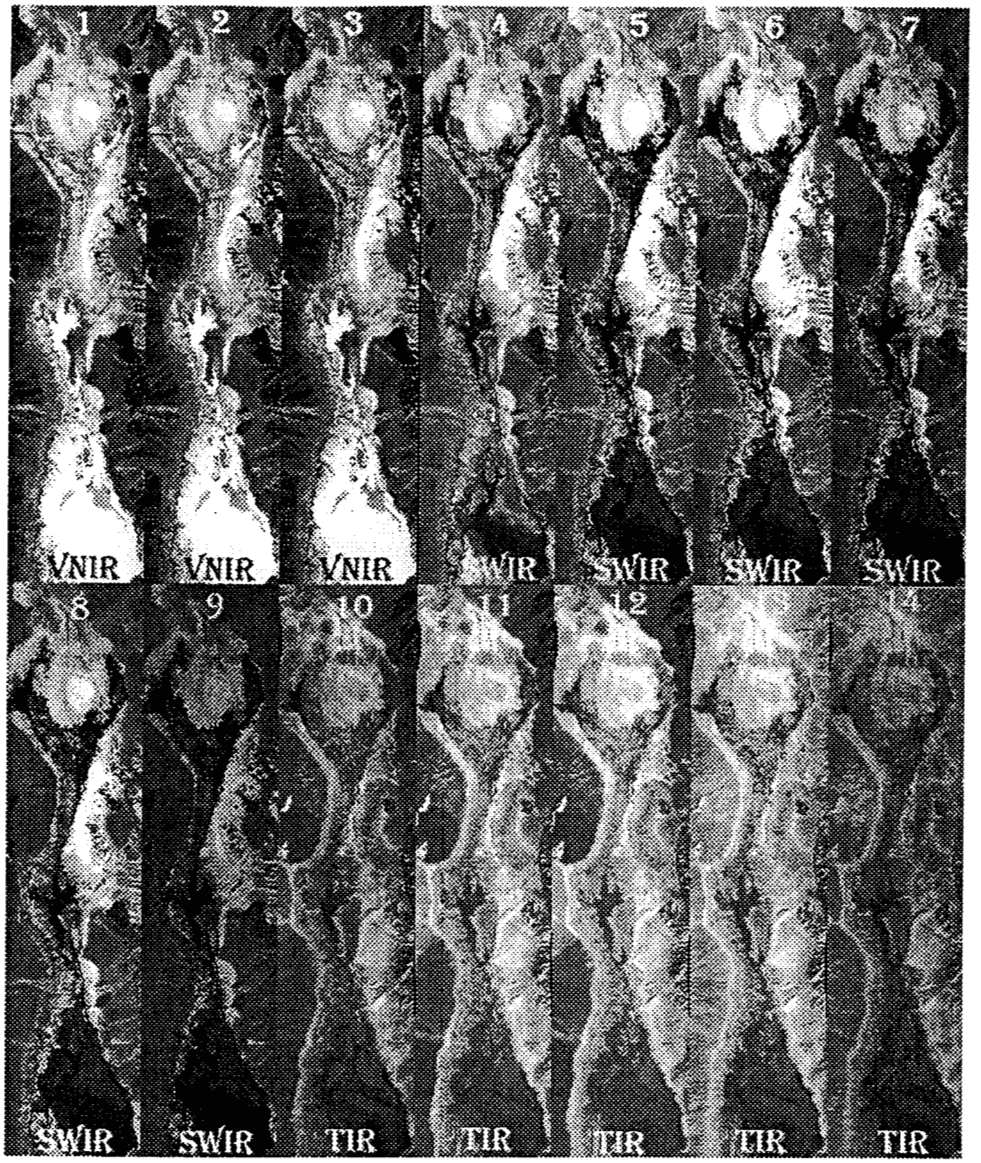

Figure 2. The 14 ASTER bands, contrast stretched for this presentation. There are three bands in the VNIR, six bands in the short wavelength infrared, and five bands in the thermal infrared (see table 1 for specifications). Each image covers an area of 12 km × 60 km.

the radiation emitted and reflected at the surface. Atmospheric corrections are necessary to isolate those features of the observation which are intrinsic to the surface, from those caused by the atmosphere. Only after accurate atmospheric correction can one proceed to study seasonal and annual surface changes and to attempt the extraction of surface kinetic temperatures and emissivities.

The approach used for atmospheric correction in the thermal infrared involves two fundamental elements: (1) the use of a radiation transfer model capable of

estimating the magnitude of atmospheric emission, absorption and scattering; and (2) the acquisition of all the necessary atmospheric parameters (e.g. temperature, water vapour, ozone, aerosol profiles) at the time and location of the measurement to be corrected.

The model used is MODTRAN2 (Abreu *et al.* 1991), a recent version of MODTRAN that traces its heritage back through the several versions of LOWTRAN (Kneizys *et al.* 1988, 1996). The second element of the atmospheric correction approach involves identifying sources for all the necessary input atmospheric parameters that are either as accurate as necessary to meet the overall accuracy goal or are the best available. Most of these parameters will be obtained from other EOS AM-1 platform instruments, or from assimilation models. The radiance product is reported in units of radiance ($W\,m^{-2}\,sr^{-1}\,\mu m^{-1}$).

3.6. *Temperature–emissivity separation*

Accurate determination of surface kinetic temperature, as opposed to brightness temperature, requires knowledge of spectral emissivity. Temperature–emissivity separation (TES) algorithms are always approximations: separation is difficult because there are five measurements but six unknowns (five temperatures and one emissivity). Various approaches have been used to constrain the extra degree of freedom. TES operates on ASTER 'land-leaving TIR radiance' data which have already been corrected for atmospheric transmission and upwelling radiance. ASTER's TES algorithm (Gillespie *et al.* 1998) hybridizes three established algorithms, first estimating the temperature by the normalized emissivity method (Gillespie 1985), and then using it to calculate unbiased emissivity band ratios. An empirical relationship (Matsunaga 1994) predicts the minimum emissivity from the spectral contrast (min–max difference or MMD) of the ratioed values (Watson 1992), permitting recovery of the emissivity spectrum. TES uses an iterative approach to remove reflected sky irradiance. Based on numerical simulation, TES can recover temperatures within about ± 1.5 K, and emissivities within about ± 0.015. Limitations arise from the empirical relationship between emissivity values and spectral contrast, compensation for reflected sky irradiance, and ASTER's precision, calibration, and atmospheric correction. Output products are:

Surface kinetic temperature is a single image plane consisting of short-integer (16-bit) pixels specifying the temperature in quanta of 0.1 K. Output is T multiplied by 10 (figure 3(*A*) and (*B*).

Surface emissivity is coded in five image planes consisting of 16-bit pixels specifying the emissivity in quanta of 0.001. Output is multiplied by 1000. The possible emissivity range of 0–1 is thus encoded as 0–1000 (figure 4(*A*) and (*B*)).

3.7. *Digital Elevation Model*

The ASTER stereoscopic subsystem consists of nadir and rear-viewing telescopes operating in the VNIR wavelengths (band 3). This subsystem, configured to provide a base-to-height ratio of 0.6, will acquire along-track, digital stereo data at 15 m resolution over a 60 km ground swath. Digital Elevation Models (DEMs) will be produced, after launch of the EOS AM platform (Welch *et al.* 1998), from either ASTER Level 1A or 1B input data (figure 5).

A digital stereo correlation approach will be used to calculate parallax differences and derive DEMs from ASTER stereo pairs. ASTER standard product DEM production will use commercial off-the-shelf photogrammetric software and hardware that

Figure 3. Temperature image produced by temperature–emissivity separation algorithm. (*A*) Black and white, contrast-enhanced depiction of temperature, with warmer temperatures displayed in lighter shades; (*B*) colour-coded version of (A) showing temperatures ranging from 32° C (black) to 62° C (white).

implement the procedure. A commercial system will be acquired and operated to produce the DEM standard data product at a rate of one scene per day, starting soon after launch.

The process for generating DEMs starts with the construction of a stereo pair by registering two images of the same ground area recorded from different positions in space. In the stereo pair, any positional differences parallel to the direction of satellite travel (parallax differences) are attributed to displacements caused by relief. Relative ground elevations are determined by measuring parallax differences in the

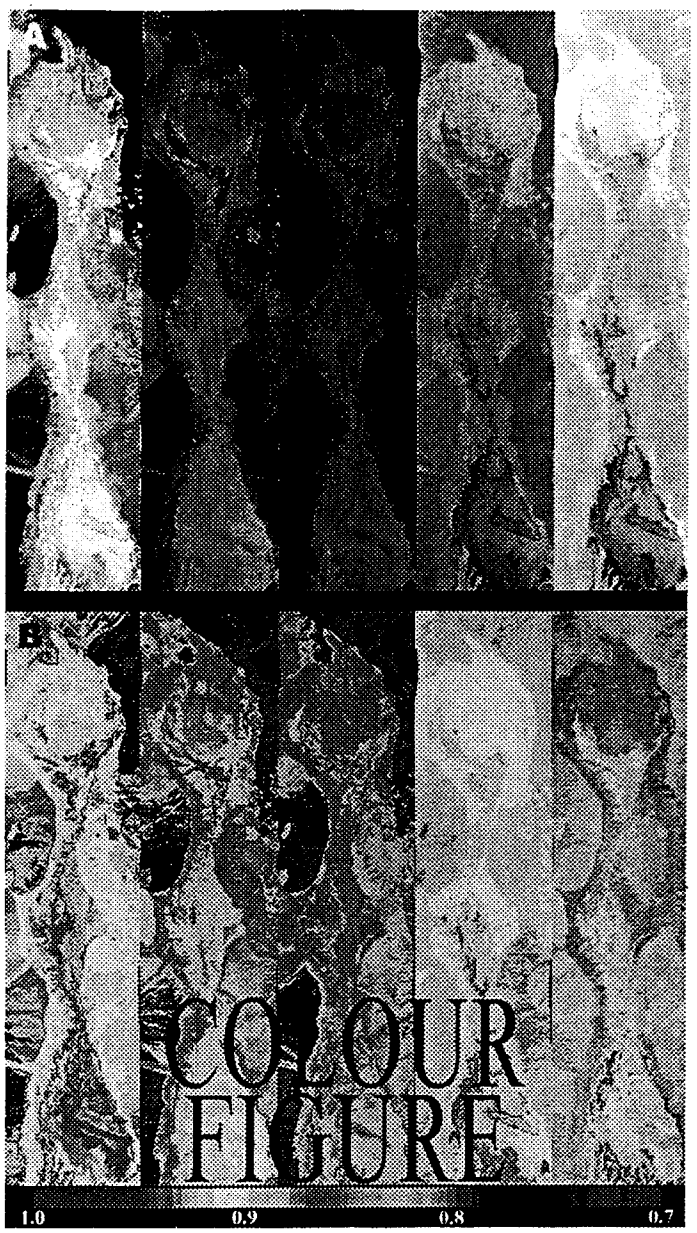

Figure 4. Five emissivity channels from ASTER bands 10–14, produced by temperature–emissivity separation algorithm. (*A*) Black and white portrayal of emissivity values, with higher emissivity values displayed in lighter shades; (*B*) colour-coded version of (A) showing emissivity values ranging from 0.7 (black) to 1.0 (red) for each of the five TIR channels.

registered images. True or absolute elevations (Z-coordinates) are determined in a subsequent step.

DEM accuracies depend on the presence or absence of Ground Control Points (GCPs), provided by a data requester. In the absence of GCPs, the relative DEM will have an accuracy of 15–30 m. The availability of accurate GCPs will allow

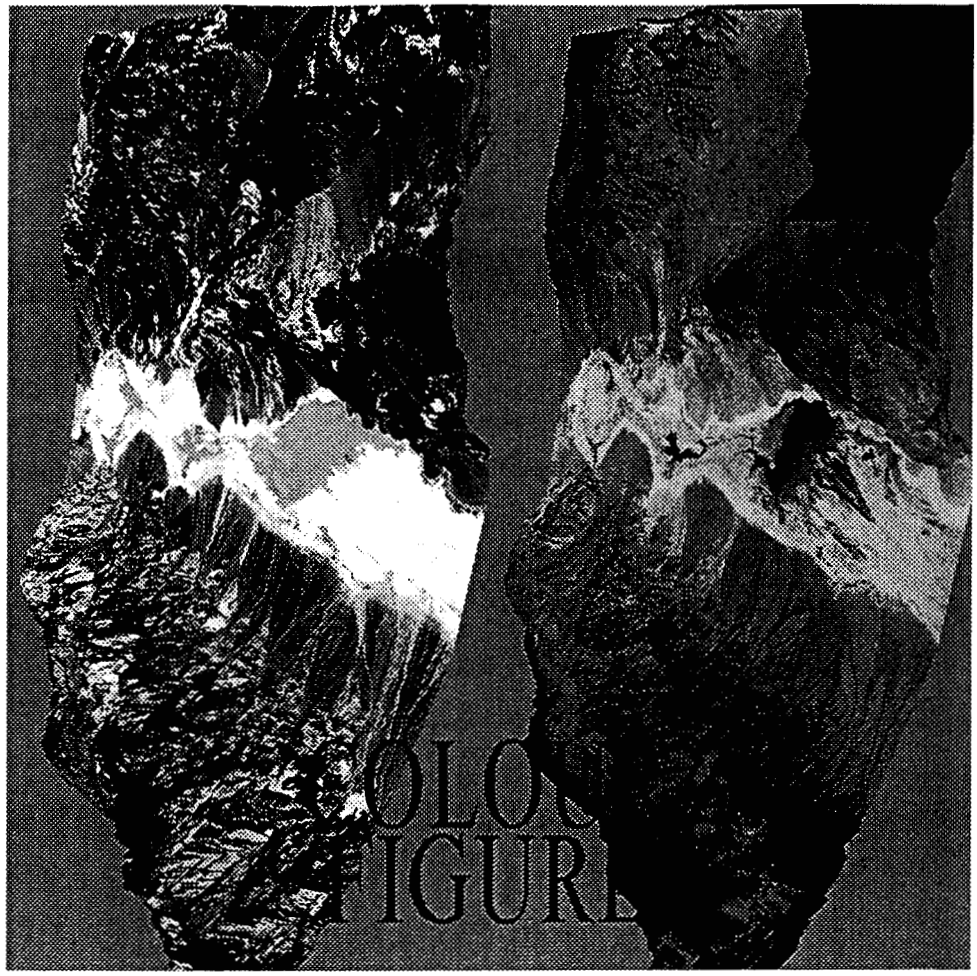

Figure 5. Perspective views of Death Valley, California produced by draping simulated ASTER image data over Digital Elevation Model data. The top image displays ASTER bands 6, 3 and 1 in red, green and blue; the bottom uses ASTER TIR bands 14, 12 and 10 displayed in red, green and blue. The images cover a full 60 km × 60 km ASTER scene.

production of absolute DEMs with accuracies depending on the number and quality of control points (table 3).

ASTER DEMs can be combined with image data to produce 3-D perspective views or visualizations. Examples for Death Valley are shown in figure 4, where a

Table 3. DEM accuracies as a function of GCPs.

Product name	No. of GCPs (minimum)	GCP (rms. *Exyz*) accuracy (m)	DEM (rms. *Exyz*) accuracy (m)
Relative DEM	0	N/A	10–30
Absolute DEM	1	15–30	15–50
Absolute DEM	4	5–15	7–30

visible and infrared composite is draped over a DEM (top) and a TIR composite is draped over a DEM (bottom).

4. Obtaining ASTER data

ASTER data will be available through EOSDIS by using an on-line web-based search and order tool. Any data that have already been acquired are available to all by submitting a Data Processing Request (DPR). A data processing request is submitted via the Version 0 Information Management (V0 IMS) tool. This tool allows the user to search the database of ASTER scenes to determine if data have been acquired over the user's study area. If data have been acquired the tool allows the user to order the data. However, ASTER is also an on-demand instrument. This means data will only be acquired over a location if a Data Acquisition Request (DAR) has been submitted. Registered users can submit a data acquisition request via the Data Acquisition Request Tool. In order to use this tool users must first register and receive approval from a committee consisting of NASA Headquarters officials, ASTER Science Team members, and other scientists. For more information please visit the ASTER web site at http://asterweb.jpl.nasa.gov

5. Conclusions

The ASTER instrument is the logical follow-on to the Landsat TM instrument in regards to extending the capabilities of a global data acquisition, high spatial resolution imager. ASTER will be the first satellite imager to obtain multispectral thermal infrared data and simultaneously acquired high resolution stereo data. Data will be available to everyone through a web-based search and order system. In addition, approved investigators will be able to command the instrument to acquire specific data for their individual investigations, tailoring the instrument configuration to their viewing needs. In this regard, ASTER is unique; and it will provide the earth science community with an unparalleled set of data for scientific research.

Acknowledgements

This work was performed at the California Institute of Technology/Jet Propulsion Laboratory under contract to the National Aeronautics and Space Administration. Thanks to Simon Hook for helpful suggestions.

References

ABRAMS, M., and HOOK, S., 1995, Simulated ASTER data for geologic studies. *IEEE Transactions on Geoscience and Remote Sensing*, **33**, 692–699.

ABREU, L., KNEIZYS, F., ANDERSON, G., CHETWYND, J., BERK, A., BERNSTEIN, L., and ROBERTSON, D., 1991, MODTRAN. *Proceedings 1991 Battlefield Atmospherics Conference, El Paso TX*, pp. 000–000.

BIGGAR, S., GELLMAN, D., and SLATER, P., 1990, Improved evaluation of optical depth components from Langley plot data. *Remote Sensing of Environment*, **32**, 91–101.

FUJISADA, H., 1998. ASTER Level-1 data processing algorithm. *IEEE Transactions on Geoscience and Remote Sensing*, **36**, 1101–1112.

GILLESPIE, A., KAHLE, A., and WALKER, R., 1986, Color enhancement of highly correlated images. I. Decorrelation and HSI contrast stretches. *Remote Sensing of Environment*, **20**, 209–235.

GILLESPIE, A., MATSUNAGA, T., ROKUGAWA, S., and HOOK, S., 1998, A temperature and emissivity separation algorithm for ASTER images. *IEEE Transactions on Geoscience and Remote Sensing*, **36**, 1113–1126.

GREEN, R., VANE, G., and CONEL, J., 1988, Determination of in-flight spectral, radiometric, spatial and signal-to-noise performance of Airborne Visible/Infrared Imaging

Spectrometer. *Proceedings of AVIRIS Performance Evaluation Workshop*, Jet Propulsion Laboratory Publication 88-38, Pasadena, California, pp. 162–184.

KNIEZYS, F., SHETTLE, E., ABREU, L., CHETWYND, J., ANDERSON, G., GALLERY, W., SELBY, A., and CLOUGH, S., 1988, User guide to LOWTRAN 7. Air Force Geophysics Laboratory Report No. AFGL-TR-88-0177, Hanscom AFB, Mass 0731.

KNIEZYS, F., ABREU, L., ANDERSON, G., CHETWYND, J., SHETTLE, E., BERK, A., BERNSTEIN, L., ROBERTSON, D., ACHARYA, P., ROTHMAN, L., SELBY, J., GALLERY, W., and CLOUGH, S., 1996, The MODTRAN 2/3 report and LOWTRAN 7 model, edited by L. W. Abreu and G. P. Anderson. Phillips Lab., Geophysics Directorate, PL/GPOS, Hanscom AFB, MA 01731, Contract F19628-91-C-0132.

MATSUNAGA, T., 1994, A temperature–emissivity separation method using an empirical relationship between the mean, the maximum, and the minimum of the thermal infrared emissivity spectrum. *Journal of Remote Sensing Society of Japan*, **14**, 230–241 (in Japanese with English abstract).

PALLUCONI, F., and MEEKS, G., 1985, Thermal infrared multispectral scanner (TIMS): an investigator's guide to TIMS data. Jet Propulsion Laboratory Publication 85-32, Pasadena, California.

PRICE, R., KING, M., DALTON, K., PEDELTY, P., ARDANUY, P., and HOBISH, M., 1994, Earth Science data for all: EOS and the EOS Data and Information System. *Photogrammetric Engineering and Remote Sensing*, **60**, 277–285.

SOHA, J. M., and SCHWARTZ, A., 1978, Multispectral histogram normalization contrast enhancement. *Proceedings of the 5th Canadian Symposium on Remote Sensing, Victoria, BC, Canada*, pp. 86–93.

SLATER, P., BIGGAR, S., HOLM, R., JACKSON, R., MAO, Y., MORAN, M., PALMER, J., and YUAN, B., 1987, Reflectance- and radiance-based methods for the in-flight absolute calibration of multispectral sensors. *Remote Sensing of Environment*, **22**, 11–37.QuickMark

QUICKMARKTHOME, K., GELLMAN, D., PARADA, R., BIGGAR, S., SLATER, S., and MORAN, M., 1993. In-flight radiometric calibration of Landsat-5 Thematic Mapper from 1984 to present. *Proceedings of SPIE*, **1938**, 1993.

THOME, K., HERMAN, B., and REAGAN, J., 1992, Determination of precipitable water from solar transmission. *Journal of Applied Meteorology*, **31**, 157–165.

WATSON, K., 1992, Spectral ratio method for measuring emissivity. *Remote Sensing of Environment*, **42**, 113–116.

WELCH, R., JORDAN, T., LANG, H., and MURAKAMI, H., 1998, ASTER as a source for topographic data in the late 1990s. *IEEE Transactions on Geoscience and Remote Sensing*, **36**, 1282–1289.

YAMAGUCHI, Y., KAHLE, A., TSU, H., KAWAKAMI, T., and PNIEL, M., 1998, Overview of Advanced Spaceborne Thermal Emission and Reflection Radiometer (ASTER). *IEEE Transactions on Geoscience and Remote Sensing*, **36**, 1062–1071.